

LA-UR- 04-7243

Approved for public release;  
distribution is unlimited.

*Title:* Planar velocity and scalar concentration measurements in shock-accelerated, unstable fluid interfaces

*Author(s):* C. Goodenough, S. Kumar, M. Marr-Lyon, A. Boyts, K. Prestridge, P. Rightley, C. Tomkins, M. Cannon, J. Kamm, W. Rider, C. Zoldi-Sood, G. Orlicz, P. Vorobieff

*Submitted to:* Proceedings of the SPIE 26th International Congress on High-Speed Photography and Photonics



Los Alamos National Laboratory, an affirmative action/equal opportunity employer, is operated by the University of California for the U.S. Department of Energy under contract W-7405-ENG-36. By acceptance of this article, the publisher recognizes that the U.S. Government retains a nonexclusive, royalty-free license to publish or reproduce the published form of this contribution, or to allow others to do so, for U.S. Government purposes. Los Alamos National Laboratory requests that the publisher identify this article as work performed under the auspices of the U.S. Department of Energy. Los Alamos National Laboratory strongly supports academic freedom and a researcher's right to publish; as an institution, however, the Laboratory does not endorse the viewpoint of a publication or guarantee its technical correctness.

Form 836 (8/00)



# Planar Velocity and Scalar Concentration Measurements in Shock-accelerated, Unstable Fluid Interfaces

Cherie Goodenough<sup>\*a</sup>, Sanjay Kumar<sup>a</sup>, Mark Marr-Lyon<sup>a</sup>, Adam Boyts<sup>a</sup>, Kathy Prestridge<sup>a</sup>, Paul Rightley<sup>a</sup>, Chris Tomkins<sup>a</sup>, Michael Cannon<sup>a</sup>, James Kamm<sup>a</sup>, William Rider<sup>a</sup>, Cindy Zoldi-Sood<sup>a</sup>, Greg Orlicz<sup>b</sup>, Peter Vorobieff<sup>b</sup>

<sup>a</sup>Los Alamos National Laboratory, P.O. Box 1663, Los Alamos, NM, USA 87545

<sup>b</sup>Dept. Of Mech. Eng., University of New Mexico, Albuquerque, NM, USA 87131

## ABSTRACT

We report applications of several high-speed photographic techniques to diagnose fluid instability and the onset of turbulence in an ongoing experimental study of the evolution of shock-accelerated, heavy-gas cylinders. Results are at Reynolds numbers well above that associated with the turbulent and mixing transitions. Recent developments in diagnostics enable high-resolution, planar (2D) measurements of velocity fields (using particle image velocimetry, or PIV) and scalar concentration (using planar laser-induced fluorescence, or PLIF). The purpose of this work is to understand the basic science of complex, shock-driven flows and to provide high-quality data for code validation and development. The combination of these high-speed optical methods, PIV and PLIF, is setting a new standard in validating large codes for fluid simulations. The PIV velocity measurements provide quantitative evidence of transition to turbulence. In the PIV technique, a frame transfer camera with a 1 ms separation is used to image flows illuminated by two 10 ns laser pulses. Individual particles in a seeded flow are tracked from frame to frame to produce a velocity field. Dynamic PLIF measurements of the concentration field are high-resolution, quantitative dynamic data that reveal finely detailed structure at several instances after shock passage. These structures include those associated with the incipient secondary instability and late-time transition. Multiple instances of the flow are captured using a single frame Apogee camera and laser pulses with 140  $\mu$ s spacing. We describe tradeoffs of diagnostic instrumentation to provide PLIF images.

## 1. INTRODUCTION

### 1.1. Unstable Fluid Dynamics

The Richtmyer-Meshkov (RM) instability (Meshkov<sup>1</sup>, Richtmyer<sup>2</sup>) occurs during the acceleration of material interfaces in which the density gradient and pressure gradient are misaligned. This misalignment leads to a baroclinic deposition of vorticity that distorts the interface, leading to mixing and transition to turbulence at late time. RM instability has applications in a many fields. Examples include astrophysics (Arnett *et al.*<sup>3</sup>), supersonic combustion (Yang *et al.*<sup>4</sup>) and inertial confinement fusion (Lindl *et al.*<sup>5</sup>).

### 1.2. Experimental Goals

Shock-accelerated fluid dynamics experiments using a shock tube are used both for validation of fluid simulation codes and for investigating the fundamental physics of the systems. This experiment uses a membraneless interface between diffuse gases of differing densities and laser sheet illumination to capture a two-dimensional slice of the shock-accelerated flows.

Quantitative experimental measurements of RM instabilities are not-widely available. High-resolution, quantitative estimates of velocity and vorticity fields are almost nonexistent even though the deposited vorticity is the principal mechanism driving the instability (Tomkins *et al.*<sup>6</sup>).

We use several high-speed photography techniques to achieve high resolution concentration images ( $\sim 50$   $\mu$ m/pixel), multiple concentration measurements per event, high resolution two-dimensional velocity fields and accurately measured initial flow conditions.

---

\* [goodenough@lanl.gov](mailto:goodenough@lanl.gov), phone 1 505 667-8737, fax 1 505 667-5748, [lanl.gov](http://lanl.gov)

## 2. DIAGNOSTICS

### 2.1. Gas Shock Tube

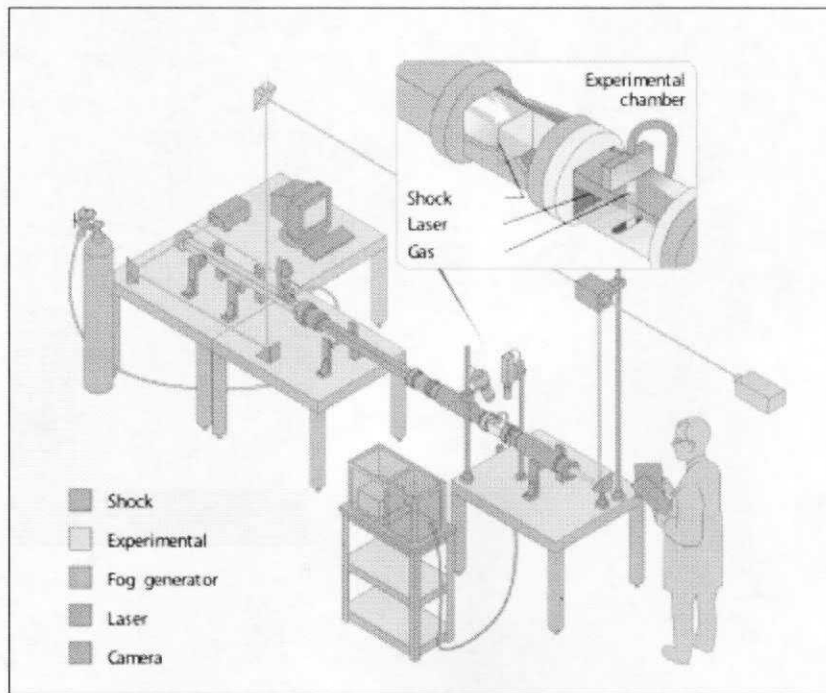


Figure 1. The LANL Gas Shock Tube Experiment

Figure 1 shows a drawing of the experimental setup. The shock tube is 5.4 m long with a square inner cross-section of 75 mm x 75 mm. The tube is instrumented downstream of the driver section with three piezoelectric pressure transducers to obtain shock speed and to trigger the lasers and cameras. The experiment is controlled with an in-house program using LabView.

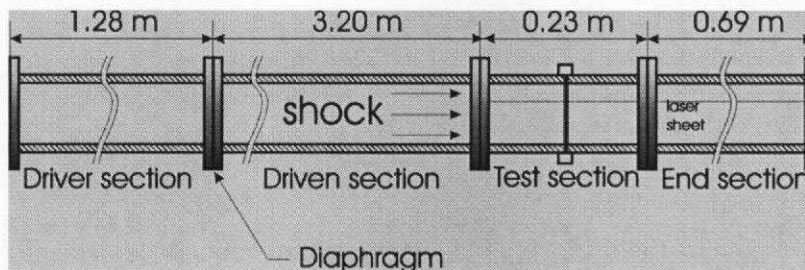


Figure 2. Side-view schematic of shock tube.

A side-view schematic of the shock tube is shown in Figure 2. The shock is generated by placing a diaphragm at the downstream end of the driver section. This section is then pressurized to 20 psig. The downstream side of the shock tube is open to atmosphere and filled with ambient air. Solenoid-driven razor blades puncture the diaphragm generating a Mach 1.2 shock wave which becomes planar as it propagates through the driven section. In the test section, the shock wave impacts a target flow of  $\text{SF}_6$ , which has a density five times that of air. Figure 3 shows a schematic of the test section.

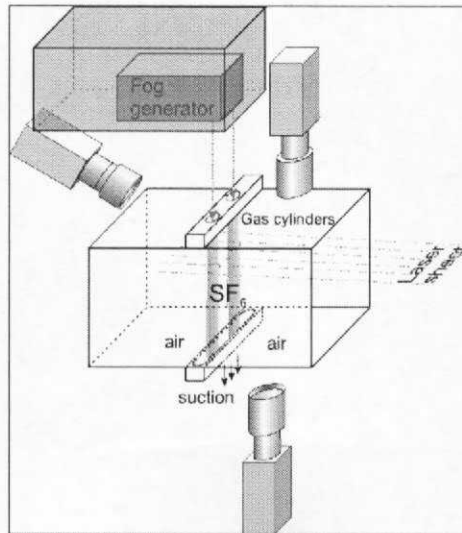


Figure 3. Schematic of shock tube test section.

The targets used are most often cylinders of  $SF_6$ , although gas curtains have been used as well. The  $SF_6$  is seeded with either fog or acetone vapor and is gravity-fed in to the test section through an orifice. This schematic shows two circular orifices used to produce two, cylindrical jets of seeded  $SF_6$ . The vertical flow velocity ( $\sim 10$  cm/s) is small compared to the speed of the shock ( $\sim 400$  m/s) or the convection velocity of the unstable flow structures ( $\sim 100$  m/s) (Tomkins *et al.*). The three cameras shown in the schematic capture images of the initial conditions (IC), dynamic concentration images (DYN) and particle image velocimetry (PIV) images to obtain two-dimension velocity information. A dynamic image of the initial conditions and first dynamic instance of a two cylinder target seeded with theatrical fog is show in Figure 4.

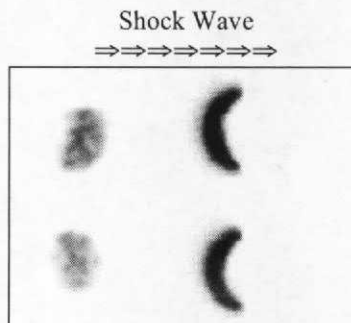


Figure 4. Initial conditions and first dynamic instance in fog-seeded  $SF_6$  cylinders.

## 2.2. Concentration Diagnostics

The goal for our concentration diagnostics is to obtain high-resolution images from which we can obtain concentration as a function of intensity on the image. We need to be able to do this both before the passage of the shock, where we have initial conditions that are diffused, and after, where we have shock-accelerated objects.

Historically, we have used theatrical fog to seed the  $SF_6$  flows. We simply flow  $SF_6$  in to a tank, inject theatrical fog particles and then gravity-feed the mixture in to the test section. We then use a doubled Nd:YAG laser (532 nm) whose beam has been formed in to a light sheet to illuminate a cross-section of the flow both before and at several instances after the passage of the shock wave. We image the scattered, green light off of the fog particles. This method is quite successful at tracking the flows after passage of the shock. However, since the fog consists of particles it does not

diffuse, while the  $\text{SF}_6$  diffuses to have a peak concentration as low as 67% at the image plane. This results in poor marking of the initial conditions by the fog. Unmarked areas remain so after shock passage.

The most direct method of obtaining concentration measurements is using the phenomenon of Rayleigh scattering (RS) of laser light off of  $\text{SF}_6$  and air molecules themselves. Since the amount of RS is proportional to the size of the molecule, this can provide direct concentration information.

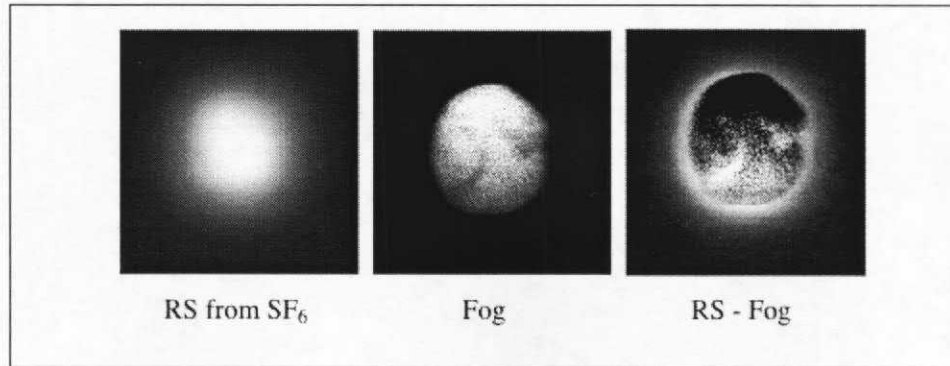


Figure 5. Comparison of Rayleigh scattering and fog concentration images for single-cylinder initial conditions.

Figure 5 shows the results of a comparison between the RS and fog methods of obtaining concentration fields. In this example of a single-cylinder target, the fog-seeded flow appears to have a sharp edge, while the image obtained using RS directly from the  $\text{SF}_6$  molecules shows significant diffusion. The RS method presents significant difficulties in its application, however. It requires either the use of a very high-power laser, or the integration of several pulses of a lower power laser. The latter is entirely unsuitable for obtaining dynamic images of shock-accelerated flows. Also, the flows must be kept very free of dust particles which will saturate the image.

The most practical method for improving concentration diagnostics has proved to be using the phenomenon of planar laser induced fluorescence (PLIF). In this technique, we bubble the  $\text{SF}_6$  through liquid acetone to saturate the flow with acetone vapor. We then use a quadrupled Nd:YAG laser light sheet (266 nm) to excite the acetone molecules. The acetone molecules then fluoresce in a broadband (350 – 550 nm). Acetone vapor has diffuses in a similar manner to  $\text{SF}_6$  so this technique provides excellent tracking of the flow both before and after shock passage.

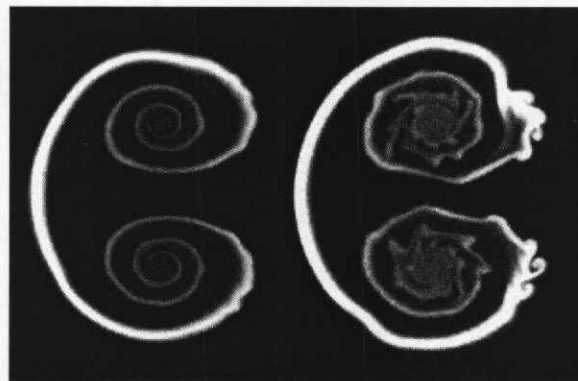


Figure 6. PLIF image of a single-cylinder after shock passage.

A PLIF image of a single-cylinder target after shock passage is shown in Figure 6. These images were obtained using an Apogee AP8P back-illuminated camera with a 2 s exposure time. Instantaneous images are obtained by using two, 10 ns pulses of a New Wave Research quadrupled Nd:YAG laser, 160  $\mu\text{s}$  apart. The  $\text{SF}_6$  target flow is a single, 8mm cylinder. The image above is 1 cm top to bottom and the shock passes from left to right.

Quantitative concentration information can be obtained from images such as the one in Figure 6. However, the procedure is rather involved and is still a work in progress. In order to calibrate the technique the bias offset of the camera must be removed using a dark-field image. Low-frequency lens/aperture effects and pixel-to-pixel variation are removed using a flat-field image. A calibration image taken with the entire shock tube filled with acetone-seeded SF<sub>6</sub> is used to remove variations in the light sheet intensity. However, the large volume of SF<sub>6</sub> between the window in to the shock tube and the target area causes exponential decay in intensity which must be removed with a fit.

### 2.3. Velocity Field Diagnostics

We obtain high-resolution, two-dimensional velocity fields of our shock-accelerated flows using a technique called particle image velocimetry (PIV). In this technique, both the flow of SF<sub>6</sub> and the background air are lightly seeded with theatrical fog particles. The usual Mach 1.2 shock wave is generated and impacts the target. After shock passage, two images are obtained using two pulses of a doubled Nd:YAG laser, 2 μs apart. The images are captured on a MegaPlus Model ES 1.0 CCD camera. The camera is used in double exposure mode with the first frame having a duration of 100 μs followed by a 1 μs buffer and finally a video frame. Obviously, timing is an issue. We use a National Instruments timing card controlled by a LabView program to pulse the laser heads and camera. Below, Figure 7 shows two partial frames of PIV data.

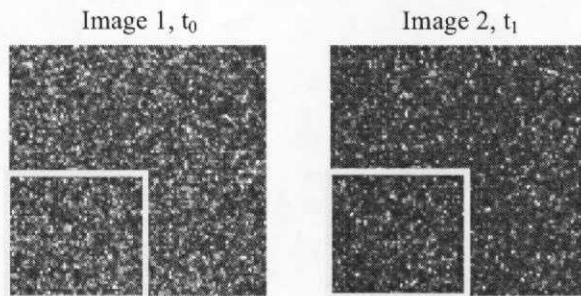


Figure 7. PIV images - SF<sub>6</sub> and background seeded with fog.

In PIV analysis, particles in small boxes in the frames are tracked from one frame to the next. A peak is found in the correlation plane corresponding to a displacement vector for the box (convection velocity of 100 m/s removed). Since the time between frames is well known, a velocity vector is obtained for each box. Our analysis enables us to obtain a resolution of 60 x 60 vectors with 187 μm spacing. The result is a high-resolution, two-dimensional velocity field as shown below in Figure 8.

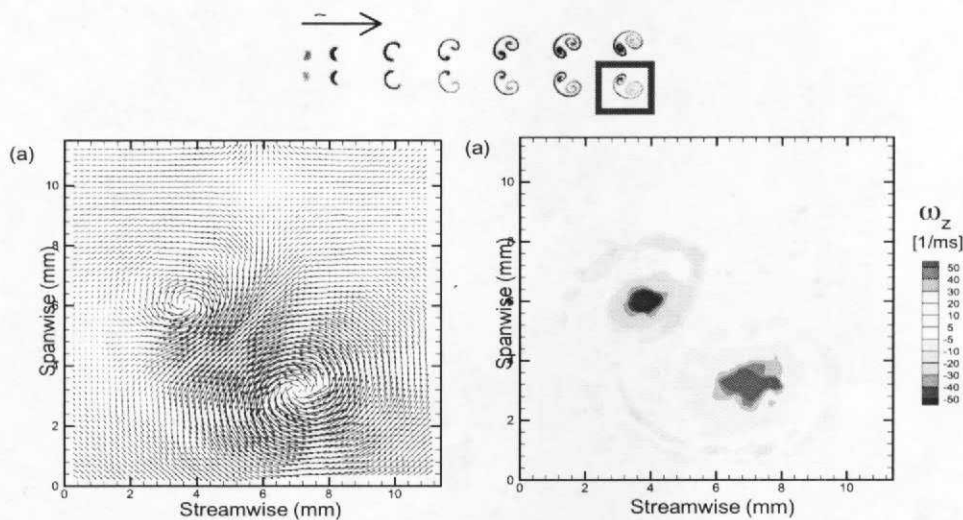


Figure 8. Velocity and vorticity field of cylinder shown in blue box.

Figure 8 also shows the vorticity field as calculated from the velocity field. Vorticity is the curl of the velocity field.

### 3. RESULTS

#### 3.1. Single Cylinder

Having obtained high-resolution velocity fields, it is possible to do a direct and quantitative analysis of a comparison between experimental results and results of simulation codes. We compared PIV results from a single-cylinder target to those arrived at using RAGE, a LANL ASCI code. Figure 9 shows a comparison of both the velocity and vorticity fields.

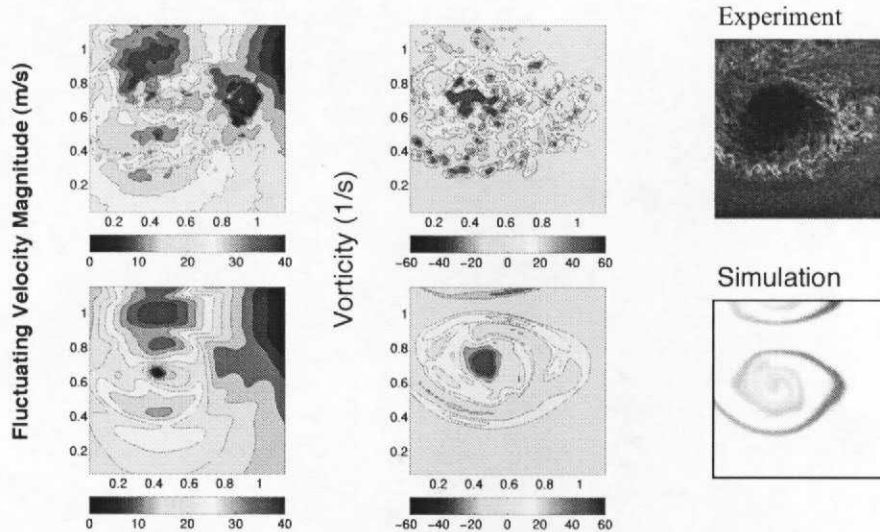


Figure 9. Velocity and vorticity fields for single vortex. Experimental and RAGE simulation data.

There is large scale agreement between the simulations and the experiment in both velocity and vorticity. However, there are clearly instabilities at smaller scales in the experiment that are not captured in the code (C. Zoldi<sup>7</sup>). This data was taken before the implementation of PLIF for initial conditions and consequently a diffusion factor of .67 had to be applied to the experimental initial conditions to get agreement.

#### 3.2. Double Cylinder

Qualitative comparisons can be made between concentration data and simulation results as well. As we move forward to quantitative PLIF there will be the opportunity for real, physics based comparisons. Figure 10 shows the improvement in tracing diffused areas of the initial flow from fog-seed to PLIF methods and their comparison to simulation results from another LANL code, Cuervo.

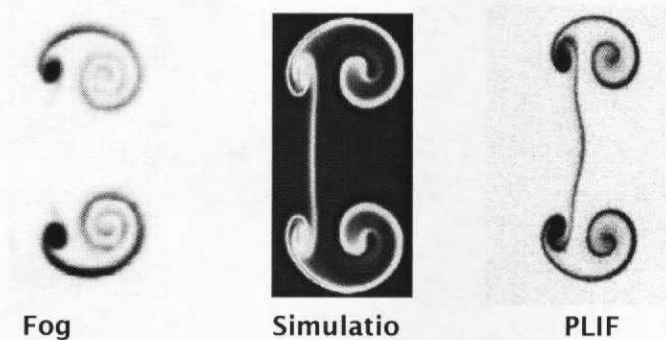


Figure 10. Concentration data from experimental fog, simulation and experimental PLIF.

It is exciting to note that the simulation result came before the experimental PLIF data. In fact, the existence of the “bridge” (the line of SF<sub>6</sub> between the vortex pairs visible in the simulation and PLIF data) was part of the motivation for moving to the PLIF method.

Once again we see large scale agreement between experiment and simulation. However, there are smaller-scale instabilities that are simply not resolved by the code.

#### 4. CONCLUSIONS

High-resolution, two-dimensional concentration and velocity fields obtainable through the application of PLIF and PIV methods have allowed direct study of shock-accelerated, unstable fluid interfaces. These techniques open the door to quantitative, physics-based comparison to simulation codes and models.

In the future, we will move toward three-dimensional characterization of the flows. It is most likely that the small scale instabilities that the simulations are not resolving arise from the inescapably three-dimensional nature of the experiment. We will also work to implement simultaneous PLIF and PIV imaging (made possible through the use of bandpass filters) to obtain simultaneous concentration and velocity fields. We are also interested in studying re-shock with these techniques.

---

<sup>1</sup> E. Meshkov, “Instability of the interface of two gases accelerated by a shock wave,” *Izv. Akad. Nauk SSSR, Mekh. Zhidk. Gaza* **4**, 151 (1969)

<sup>2</sup> R.D. Richtmyer, “Taylor instability in shock acceleration of compressible fluids,” *commun. Pure Appl. Math.* **8**, 297 (1960)

<sup>3</sup> W. Arnett, J. Bahcall, R. Kirshner, and S. Woosley, “Supernova 1987A,” *Annu. Rev. Astron. Astrophys.* **27**, 629 (1989)

<sup>4</sup> J. Yang, T. Kubota, and E.E. Zukoski, “Applications of shock-induced mixing to supersonic combustion,” *AAIAA J.* **31**, 854 (1993)

<sup>5</sup> J. Lindl, R. McCrory, and E. Campbell, “Progress toward ignition and burn propagation in inertial confinement fusion,” *Phys. Today* **45**, 32 (1992)

<sup>6</sup> C. Tomkins, K. Prestridge, P. Rightley, M. Marr-Lyon, P. Vorobieff, and R. Benjamin, “A quantitative study of the interaction of two Richtmeyer-Meshkov-unstable gas cylinders,” *Phys. Fluids A* **15**, 986 (2003)

<sup>7</sup> C. Zoldi, “A numerical and experimental study of a shock-accelerated heavy gas cylinder,” Ph.D. thesis, Department of Applied Mathematics, State University of New York at Stony Brook, 2002